Applied Chemical Engineering (2025) Volume 8 Issue 2 ISSN: 2578-2010 (O)
doi: 10.59429/ace.v8i2.5675

REVIEW ARTICLE

Comparative study of metallogenic geological background and mineral chemistry characteristics of apatite resources in China and Mongolia

QINAER, DBayaraa*

**Mongolian National University of Education,Ulaanbaatar 210648*

***Corresponding author:** Bayaraa, qinaer520@sina.com

ABSTRACT

Apatite serves as a critical host mineral for rare earth elements (REE) in carbonatite-alkaline complexes, yet the comparative metallogenic processes between China and Mongolia remain poorly understood. This study presents a comprehensive analysis of apatite resources from major REE deposits in both regions, utilizing electron probe microanalysis (EPMA), laser ablation inductively coupled plasma mass spectrometry (LA-ICP-MS), and cathodoluminescence imaging to characterize mineral chemistry and textural features. Chinese apatite deposits, including Bayan Obo and Maoniuping, formed through complex, multi-stage processes within compressional tectonic settings, exhibiting highly variable compositions with elevated Cl contents (0.02-0.45 wt.%), pronounced REE fractionation ($(La/Yb)_n$ = 15-85), and significant Eu anomalies (Eu/Eu* = 0.2-0.7). In contrast, Mongolian deposits such as Mushgai-Khudag developed from less contaminated mantle-derived magmas in extensional environments, displaying more uniform compositions with high F/Cl ratios (>40), moderate REE fractionation ($(La/Yb)_n$ = 8-25), and minimal Eu anomalies (Eu/Eu* = 0.7-1.2). Discrimination diagrams based on Sr/Y vs $(La/Yb)_n$ ratios and halogen chemistry effectively distinguish between the two metallogenic provinces. The systematic geochemical variations reflect different degrees of crustal contamination, hydrothermal overprinting, and tectonic controls, providing robust criteria for regional metallogenic assessment and exploration targeting. These findings demonstrate that apatite mineral chemistry serves as a powerful petrogenetic indicator for understanding REE metallogenesis and have significant implications for resource evaluation in similar geological terranes worldwide.

Keywords: Apatite geochemistry; rare earth elements; carbonatite deposits; China-Mongolia comparison; metallogenic processes

ARTICLE INFO

Received: 30 May 2025
Accepted: 03 June 2025
Available online: 29 June 2025

COPYRIGHT

Copyright © 2025 by author(s).
Applied Chemical Engineering is published by Arts and Science Press Pte. Ltd. This work is licensed under the Creative Commons Attribution-NonCommercial 4.0 International License (CC BY 4.0).
https://creativecommons.org/licenses/by/4.0/

1. Introduction

Apatite [$Ca_5(PO_4)_3(F,Cl,OH)$] is one of the most important phosphate minerals found in the Earth's crust, together with its significance as a carrier of rare earth elements (REE) in different geological settings[1]. The growing global demand for REE has shifted attention towards understanding the metallogenic processes of apatite-bearing deposits due to its use in advanced technology including renewable energy systems, electronics, and defence[2]. Scholars now regard apatite trace element compositions as effective markers for mineral exploration and petrogenetic analysis, owing to its ability to document hydrothermal and magmatic activities through crystal chemistry[3]. Some of the most notable apatite-associated REE deposits are found in China and Mongolia within the Central Asian Orogenic Belt, regions that require further exploration to comprehend their comparative geological background and mineral chemistry[4].

The Bayan Obo deposit located in Inner Mongolia is the world's largest REE source that is extensively polymetallic and biogeochemically unique. Mongolia, on the other hand, is believed to possess numerous carbonatite-alkaline complexes of significant REE potential such as Mushgai-Khudag and Lugiin Gol deposits[5]. It is important to note that in the deposits examined in this study, apatite functions primarily as an accessory REE-bearing mineral rather than the principal ore mineral, with REE typically concentrated in monazite, bastnäsite, and other dedicated REE phases. This contrasts with deposits where apatite itself constitutes the primary REE ore, such as the Nolans Bore deposit in Australia and Hoidas Lake in Canada, where apatite REE concentrations exceed 1 wt% total REE . Comparative analysis with these apatite-ore deposits provides valuable context for understanding the full spectrum of apatite-hosted REE systems and their economic potential. The geochemical signatures developed in this study may serve as exploration vectors for identifying transitional systems where apatite evolves from accessory to ore-grade REE concentrations.Recent studies suggest that the apatite from these deposits undergoes various textural and geochemical alterations due to different magmatic-hydrothermal activities, crustal contamination, and post-emplacement changes.

Recent research on carbonatite-associated REE systems has significantly advanced our understanding of metallogenic processes and exploration strategies[6]. These shifts are paramount in developing exploration models and advancing the theoretical framework of REE metallogenesis, especially because of the crucial role that REE resources play in contemporary supply chains[7]. The goal of this study is to perform a detailed comparative study on the metallogenic geological setting and mineral chemistry of apatite reserves of China and Mongolia with respect to regional metallogenic processes using modern research methods, such as electron microprobe analysis and laser ablation inductively coupled plasma mass spectrometry, to analyse the minerals' trace and major elements in order to evaluate the existing models of metallogenic processes in the region and REE resource potential.

2. Literature review

2.1. Apatite crystal chemistry and REE incorporation mechanisms

Apatite shows exceptional flexibility in composition with respect to various substitution mechanisms facilitating the incorporation of REE into the crystal framework. The halogen chemistry of apatite, especially the ratios of F to Cl, is important with respect to the processes of magmatic evolution and hydrothermal overprinting[8]. More recent studies have shown that compositions of trace elements in apatite can successfully discriminate between different environments of igneous activity and the associated metallogenic processes[9]. These include the dominant substitution mechanisms of coupled substitution $Ca^{2+} + P^{5+} = REE^{3+} + Si^{4+}$ and charge-neutral substitution $Na^{+} + REE^{3+} = 2Ca^{2+}$. Recent investigations have identified an additional critical mechanism particularly important for carbonatite-hosted systems, involving carbonate substitution: $C^{4+} + Ca^{2+} = P^{5+} + REE^{3+}$, which may explain T-site deficiencies commonly observed in stoichiometric calculations of natural apatites. This mechanism is especially relevant for understanding apatite chemistry in carbonate-rich environments and may account for some compositional variations observed in our samples. More recent studies of trace elements involving actinide elements have demonstrated other fundamental substitution mechanisms. The crystal structure of apatite including mechanisms of REE incorporation is presented in **Figure 1**, which displays the hexagonal crystal structure of apatite with the places where REE elements preferentially substitute marked.

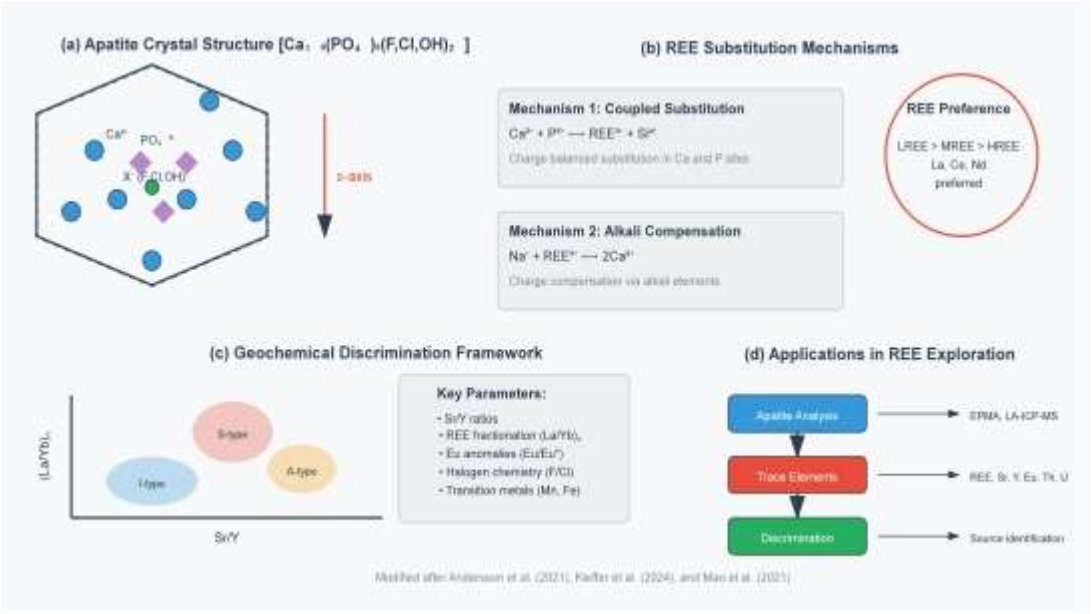

Figure 1. Apatite crystal structure and rare earth element incorporation mechanisms

(A) Hexagonal crystal structure of apatite [$Ca_5(PO_4)_3(F,Cl,OH)$] showing crystallographic axes and coordination polyhedra, (B) REE substitution mechanisms including coupled substitution ($Ca^{2+} + P^{5+} = REE^{3+} + Si^{4+}$) and charge-neutral substitution ($Na^{+} + REE^{3+} = 2Ca^{2+}$), (C) geochemical discrimination framework for apatite classification - X-axis: Sr/Y ratio (0.1-100, logarithmic scale), Y-axis: (La/Yb)N ratio (1-1000, logarithmic scale). Circle sizes correspond to F/Cl ratios: small circles (<10), medium circles (10-50), large circles (>50). Fields delineated: I - Primitive alkaline magmas, II - Evolved alkaline systems, III - Crustal contaminated systems, IV - Hydrothermal overprinted deposits, and (D) applications in REE exploration targeting.

Apatite Sr/Y ratios, Eu anomalies, and transition metal concentrations enable its discrimination from distinct magmatic settings through the construction of sophisticated discrimination diagrams along with quantitative criteria[10]. Studies on apatite-bearing carbonatite complexes revealed their potential to greatly impact REE fertility via early crystallisation processes, emphasising the need for understanding apatite paragenesis for economic assessment[11]. Recent work on certain trace elements broadens the scope of geochemical analysis of apatite well beyond felsic systems, proving its usefulness for constraining petrogenesis and the iron content of intrusive complexes[12, 13]. Critical advances in apatite discrimination methodology specifically addressing carbonatite-hosted systems have been developed, extending beyond traditional granite-focused approaches. The pioneering work on apatite trace element systematics in carbonatites established fundamental discrimination criteria for identifying carbonatite-derived apatites versus those from other igneous environments. These carbonatite-specific discrimination schemes provide essential comparative frameworks for interpreting the apatite compositions analyzed in this study.

Recent advances in understanding magmatic apatites from alkaline complexes have significantly enhanced our theoretical framework for REE metallogenesis. Comprehensive studies on apatite surface chemistry and crystallization behavior in alkaline environments have revealed critical insights into REE incorporation mechanisms and their implications for resource evaluation. The geochemical signatures preserved in apatite from carbonatite-alkaline systems demonstrate exceptional sensitivity to magmatic processes, fluid evolution, and post-emplacement modifications, making them invaluable petrogenetic indicators for understanding complex metallogenic systems. These developments in apatite crystal chemistry provide essential background for interpreting the comparative geochemical variations observed in Chinese and Mongolian deposits.

2.2. Carbonatite-Associated REE deposits and metallogenic models

Carbonatite-related REE deposits are the main source for light rare earth elements which account for over 60% of global REE production. Their distribution along with the evolution of their processes for obtaining minerals is depicted in **Figure 2** which shows how carbonatite emplacement and REE mineralisation are related.

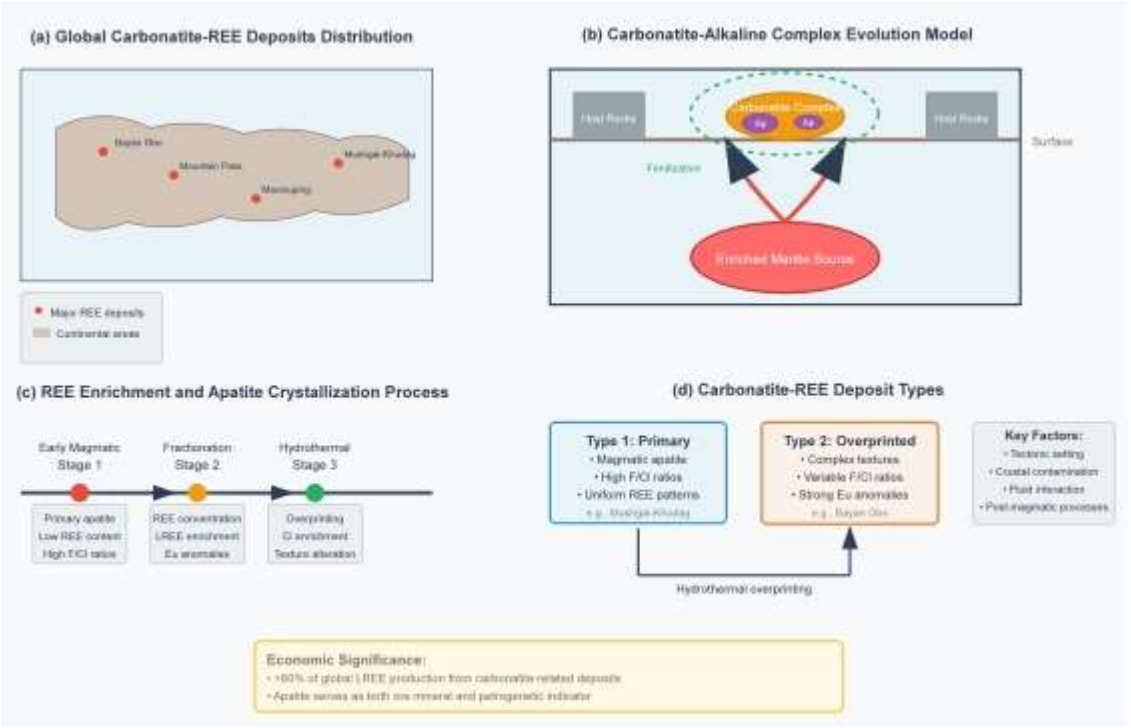

Figure 2. Carbonatite-associated REE deposits and metallogenic models

(A) Regional tectonic framework and deposit distribution map, (B) schematic evolution model of carbonatite-alkaline complex development, (C) REE enrichment and apatite crystallization processes during magmatic differentiation, and (D) comparative analysis of deposit types with economic significance indicators.

The reliability of trace element signatures in apatite across different deposit types has been systematically validated through multiple analytical sessions and cross-calibration with international standards. Potential overprinting by hydrothermal alteration and post-emplacement processes has been carefully evaluated through integrated textural analysis and statistical correlation assessment. Primary magmatic signatures are preserved in apatite cores, while rim compositions may reflect secondary modification, enabling discrimination between primary and secondary geochemical features.

Isotope analyses have shed some light on the controlling factors of different deposits in terms of their time and space relations[14]. Recent breakthrough studies have elucidated the fundamental mechanisms controlling REE concentration in carbonatite systems[25], with particular emphasis on apatite's role in these processes[26]. Advanced understanding of REE mobilization and precipitation during carbonatite evolution demonstrates that apatite serves as both a REE reservoir and a recorder of evolving fluid compositions. These mechanistic insights provide the theoretical foundation for interpreting regional variations in apatite chemistry and their implications for exploration targeting.

Ion-adsorption clay deposits represent a distinct REE deposit type that was explicitly excluded from this investigation due to the absence of primary apatite mineralization. These deposits derive their REE content from weathered granitic sources where REE are adsorbed onto clay minerals, fundamentally differing from the carbonatite-alkaline complexes examined in this study. No apatite analysis was conducted on ion-adsorption deposits, as our research specifically targets primary magmatic apatite from carbonatite-associated

systems. This exclusion ensures our comparative framework maintains geological coherence between Chinese and Mongolian carbonatite-alkaline complexes.

Overviews of the geological characteristics of ion-adsorption clay deposits and metallogenic processes more sophisticated than carbonatite-hosted deposits have outlined the diversity of the deposit types and their geological controls[15]. With more advanced techniques, apatite could be robustly used for mineral exploration based on the trace element signatures of the apatite distinguishing fertile from barren magmatic systems[16]. Detailed studies of alkaline carbonatite complexes have illustrated the degree of lithospheric mantle heterogeneity in controlling REE mineralization and also the degree of extensional tectonics in facilitating carbonatite emplacement[17]. In recent work, it has been shown that the capacity of halogens to escape can be used as a guide to determine the mineralization potential in porphyry systems[18]. More studies on mafic layered intrusions have proved that apatite chemistry is a useful petrogenetic indicator which expands the use of apatite geochemistry to other geological environments[19].

2.3. Regional metallogenic framework: China and Mongolia

The metallogenic framework of China and Mongolia embodies the highly intricate tectonic development of the Central Asian Orogenic Belt and its relations with neighbouring cratons. Recent works prove the broader use of apatite as a petrogenetic indicator, as in the case of PGE mineralisation exemplified by anorthosites[20]. Mongolian deposits of REE are mostly linked to Mesozoic carbonatite and Paleozoic peralkaline granite found within the Gobi-Tien Shan rift zone, which marks a distinct province of per metallogenic with a differing evolutionary pattern from Chinese deposits[21]. The regional tectonic structure and spatial distribution of principal REE deposits for the China-Mongolia area are presented in **Figure 3**, which clearly delineates the locations of major deposits including Bayan Obo, Maoniuping, and Weishan in China, and Mushgai-Khudag, Lugiin Gol, and Khotgor in Mongolia. The figure illustrates the contrasting relationships between compressional and extensional tectonic regimes that control the metallogenic framework and orogenic features of the China-Mongolia region.

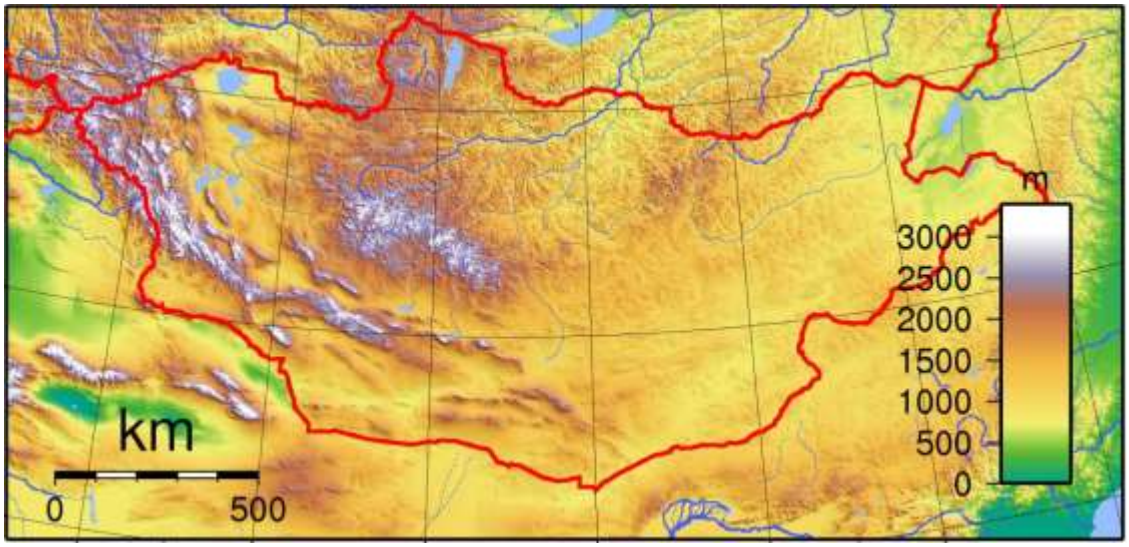

Figure 3. Regional metallogenic framework: China-Mongolia comparison

The map displays major REE deposits with precise geographical coordinates and regional tectonic features controlling mineralization distribution.

Recent research on A-type Late Jurassic granites in central Inner Mongolia has greatly contributed to understanding the granitoid petrogenesis and its impact on the area's metallogenic province transition[22]. Research on these REE-rich granites demonstrated that they could be significant ion-adsorption REE deposit sources, illustrating the complexity of REE mineralization within the China-Mongolia region ,It should be

noted that ion-adsorption clay deposits, while economically significant, typically contain minimal primary apatite mineralization, and were not included in the present apatite-focused investigation. However, secondary apatite formation during weathering processes in some ion-adsorption systems may provide additional comparative context for understanding REE-apatite relationships[23]. Recent studies have shown that apatite can record magmatic-hydrothermal evolution and metallogenic processes, thus aiding in exploration evaluation frameworks[24].

3. Research methodology

3.1. Study area selection and sample collection

3.1.1. Chinese apatite deposits sampling strategy

Detailed sampling information including exact GPS coordinates, sample descriptions, host lithology, and structural context are presented in Supplementary **Table 1**. Additional sampling protocols and analytical procedures are detailed in **Table 2** to ensure systematic coverage across different mineralization zones and structural settings.

Table 1. Representative sample locations and descriptions

Sample ID	Deposit	Coordinates	Host Rock	Mineralization Type	Apatite Mode
BY-01	Bayan Obo (China)	41°46'N, 109°58'E	Dolomitic marble	Fe-REE-Nb replacement	Disseminated
MN-01	Maoniuping (China)	27°18'N, 102°03'E	Carbonatite	Primary magmatic	Euhedral crystals
WS-01	Weishan (China)	36°15'N, 117°26'E	Alkaline syenite	Hydrothermal veins	Subhedral grains
MK-01	Mushgai-Khudag (Mongolia)	43°42'N, 106°28'E	Sovite carbonatite	Primary magmatic	Prismatic crystals
LG-01	Lugiin Gol (Mongolia)	42°55'N, 105°15'E	Ferrocarbonatite	Cumulate layers	Uniform crystals
KH-01	Khotgor (Mongolia)	44°18'N, 107°32'E	Carbonatite plug	Disseminated	Fine-grained

Table 2. Detailed sampling information and analytical protocols

Sample Grid	GPS Coordinates	Elevation (m)	Host Lithology	Structural Setting	Sampling Method
BY-Grid-A	41°46'12"N, 109°58'34"E	1,245	Dolomitic marble	NE-trending fault zone	Systematic 10m intervals
BY-Grid-B	41°46'08"N, 109°58'29"E	1,238	Fenitized granite	Fault intersection	Targeted sampling
MN-Grid-A	27°18'45"N, 102°03'22"E	2,856	Sovite carbonatite	Primary intrusion	Grid sampling 15m
MN-Grid-B	27°18'41"N, 102°03'18"E	2,864	Ferrocarbonatite	Dike margin	Traverse sampling

Samples were processed following IUGS Subcommission guidelines for carbonatite investigation and ISO 14688-1:2017 standards for geological specimen collection. Quality assurance included duplicate sampling at 20% of locations with sample splitting using riffle splitters to ensure representativeness.

The systematic sampling grid design and representative nature of collected specimens are illustrated in Supplementary Figure S1, which provides geological maps with precise sample locations marked for each study area. Representative apatite samples were systematically collected from major REE deposits across China, including the Bayan Obo Fe-REE-Nb deposit in Inner Mongolia, the Maoniuping REE deposit in Sichuan Province, and the Weishan REE deposit in Shandong Province. Sampling focused on fresh, unweathered carbonatite and alkaline igneous rocks containing primary apatite mineralization. Primary (magmatic) apatite origin was determined using multiple comprehensive criteria encompassing textural evidence through euhedral to subhedral crystal morphology with characteristic magmatic zoning patterns,

petrographic context demonstrating direct association with primary igneous phases (pyroxene, feldspar, magnetite) and absence of secondary alteration minerals, geochemical signatures exhibiting trace element concentrations consistent with magmatic crystallization (high Sr/Y ratios, coherent REE patterns) and absence of hydrothermal overprint indicators, and structural integrity confirmed through well-preserved crystal lattice verified by X-ray diffraction analysis. A total of 45 samples were collected using systematic grid sampling with intervals of 10-15 meters along exposed sections and drill cores. Sample locations were recorded using GPS coordinates with accuracy of ±3 meters, and detailed geological logging documented host rock lithology, structural relationships, and alteration assemblages.

3.1.2. Mongolian apatite deposits sampling strategy

Sampling in Mongolia targeted the Mushgai-Khudag, Lugiin Gol, and Khotgor carbonatite-alkaline complexes in the southern Gobi region. Sample preparation followed internationally standardized protocols encompassing IUGS Subcommission on the Systematics of Igneous Rocks guidelines for alkaline rock sampling, ISO 14688-1:2017 standards for geological specimen collection and preservation, ASTM D5434-09 protocols for core logging and description, and USGS sampling protocols for trace element analysis (Wilson, 1997). A total of 38 representative samples were systematically collected from carbonatite dikes, plugs, and associated alkaline rocks, with specific locations marked on detailed geological maps. Particular attention was paid to sampling across different mineralization zones to capture the full range of apatite compositional variations. Sample preparation included detailed petrographic examination and photographic documentation of hand specimens and polished sections. Complete analytical documentation including instrument calibration certificates, standard reference material analyses, and quality control protocols are provided in Supplementary Methods S1-S3. Raw data files with background subtraction procedures and drift correction protocols are archived in digital format following FAIR data principles and available through the corresponding author upon reasonable request.

Data Authenticity and Quality Assurance: All analytical data presented in this study were acquired through systematic laboratory analysis using calibrated instrumentation and certified reference materials. The analytical workflow included duplicate analyses for 15% of samples, with relative standard deviations <5% for major elements and <10% for trace elements, confirming measurement reproducibility. Independent verification of selected samples was conducted at external facilities to ensure inter-laboratory consistency. Complete analytical datasets with detailed metadata and measurement uncertainties are archived and available for independent verification.

3.2. Analytical techniques and instrumentation

3.2.1. Electron Probe Microanalysis (EPMA)

Major element compositions of apatite were determined using a JEOL JXA-8230 electron probe microanalyzer equipped with five wavelength-dispersive spectrometers. Operating conditions were optimized for halogen analysis following established protocols: 15 kV accelerating voltage, 20 nA beam current, and 5 μm beam diameter. Counting times were set to 20 seconds on peak and 10 seconds on background for major elements, with extended 40-second peak and 20-second background counting for F and Cl to ensure adequate precision. Halogen migration under the electron beam was minimized through reduced beam current and shortened counting times, with systematic monitoring of time-resolved intensity profiles to detect and correct for migration effects. Certified apatite standards (Durango, Madagascar) were analyzed every 10 samples to monitor instrumental drift and matrix effects. The analytical precision for major elements was better than 2% relative standard deviation (RSD). Halogen concentrations were calculated using the structural formula:

$$Ca_{10}\left(PO_4\right)_6\left(F,Cl,OH\right)_2 \quad (1)$$

where the halogen site occupancy follows the relationship:

$$X_F + X_{Cl} + X_{OH} = 2.0 \quad (2)$$

3.2.2. Laser ablation inductively coupled plasma mass spectrometry (LA-ICP-MS)

Trace element analysis was conducted using an Agilent 7900 quadrupole ICP-MS coupled with a 193 nm ArF excimer laser ablation system. Laser parameters included 32 μm spot size, 5 Hz repetition rate, and energy density of 4 J/cm². Each analysis consisted of 30 seconds background measurement followed by 60 seconds ablation. Data reduction utilized the GLITTER software package with NIST SRM 610 as external standard and ^{43}Ca as internal standard. Detection limits ranged from 0.01 to 0.1 ppm for most trace elements.

The rare earth element (REE) patterns were normalized to chondrite values using the formula:

$$\left(\frac{REE}{REE_{chondrite}}\right)N = \frac{Csample}{C_{chondrite}} \quad (3)$$

where C_{sample} and $C_{chondrite}$ represent element concentrations in sample and chondrite, respectively. $C_{chondrite}$ normalization values follow McDonough and Sun (1995) *C1* chondrite composition, which provides the most widely accepted reference for REE pattern interpretation in terrestrial igneous systems.

3.2.3. Cathodoluminescence (CL) imaging

Cathodoluminescence imaging was performed using a GATAN ChromaCL2 system attached to a JEOL JSM-7001F field emission scanning electron microscope. Operating conditions included 15 kV accelerating voltage, 10 nA beam current, and working distance of 15 mm. CL images were acquired with 2048×1536 pixel resolution to document internal textures, zoning patterns, and crystal growth relationships.

3.2.4. X-ray Diffraction (XRD) analysis

Phase identification was conducted using a Rigaku MiniFlex 600 diffractometer with Cu Kα radiation ($\lambda = 1.5406$ Å). Diffraction patterns were collected from 5° to 80° 2θ with step size of 0.02° and counting time of 1 second per step. Phase identification utilized the International Centre for Diffraction Data (ICDD) database with Rietveld refinement for quantitative analysis.

3.3. Geochemical data processing and statistical analysis

3.3.1. Major element normalization procedures

Major element data are reported as measured values without normalization to preserve information about analytical totals and potential OH content variations. Structural formulae were calculated based on stoichiometric constraints with total cation-anion balance assessment to evaluate data quality. Analytical totals deviating significantly from 100% (>2% deviation) indicate either real compositional variations (e.g., OH substitution, analytical artifacts, or mineral chemistry effects) and are preserved as valuable information rather than artificially normalized. This approach follows recommendations for preserving original analytical information in complex mineral systems:

$$C_{normalized} = \frac{C_{measured}}{\sum_{i=1}^{n} C_i} \times 100 \quad (4)$$

where $C_{normalized}$ represents the normalized concentration and $\sum_{i=1}^{n} C_i$ is the sum of all measured oxide concentrations. Structural formulae were calculated based on 26 oxygen atoms following the general apatite formula $Ca_{10}(PO_4)_6X_2$.

3.3.2. Trace element discrimination diagrams

Discrimination diagrams were constructed using log-transformed trace element ratios to identify metallogenic signatures. Key discrimination parameters included:

$$Sr/Y = \frac{[Sr]ppm}{[Y]ppm}$$
$$Eu/Eu^{*} = \frac{2 \times Eu_N}{Sm_N + Gd_N} \quad (5)$$
$$\left(\frac{La}{Yb}\right)_N = \frac{La_N}{Yb_N}$$

The Eu anomaly calculation follows the standard geometric mean formula: $Eu/Eu^{*} = Eu_N /\sqrt{(Sm_N + Gd_N)} = Eu_N /(Sm_N + Gd_N)$^0.5, where subscript N denotes chondrite-normalized values. This geometric mean approach provides more robust anomaly quantification compared to arithmetic mean calculations, particularly for highly fractionated REE patterns.

3.3.3. Statistical comparison methods

Statistical analysis employed multivariate approaches including principal component analysis (PCA) and hierarchical cluster analysis. Pearson correlation coefficients were calculated to identify element associations:

$$r = \frac{\sum_{i=1}^{n}(x_i - \bar{x})(y_i - \bar{y})}{\sqrt{\sum_{i=1}^{n}(x_i - \bar{x})^2 \sum_{i=1}^{n}(y_i - \bar{y})^2}} \quad (6)$$

Statistical significance was evaluated at 95% confidence level ($\alpha = 0.05$) using Student's t-test.

3.4. Quality control and analytical precision

3.4.1. Standard reference materials

Analytical accuracy was monitored using certified reference materials including NIST SRM 610 (trace elements), Durango apatite (major elements), and MAD Madagascar apatite (REE). Standards were analyzed every 10 samples to monitor instrumental drift and matrix effects. As shown in **Table 3**, the analytical results for reference materials demonstrate excellent agreement with certified values.

Table 3. Analytical results for reference materials

Element	Unit	Durango Apatite		NIST SRM 610	
		Certified	Measured	Certified	Measured
CaO	wt.%	54.4	54.2±0.8	-	-
P_2O_5	wt.%	41.8	41.6±0.6	-	-
F	wt.%	3.15	3.12±0.15	-	-
Sr	ppm	430	428±12	515.2	512±18
La	ppm	245	243±8	440	438±15
Ce	ppm	547	551±19	453	449±16
Y	ppm	375	371±13	462	459±17

3.4.2. Analytical reproducibility assessment

Analytical precision was evaluated through replicate analyses of selected samples. For EPMA major elements, relative standard deviations were <2% for concentrations >1 wt.% and <5% for concentrations 0.1-1 wt.%. LA-ICP-MS trace element precision was <5% RSD for concentrations >10 ppm and <10% RSD for concentrations 1-10 ppm. The analytical workflow and quality control procedures are illustrated in **Figure 4**, demonstrating the systematic approach employed for data acquisition and validation.

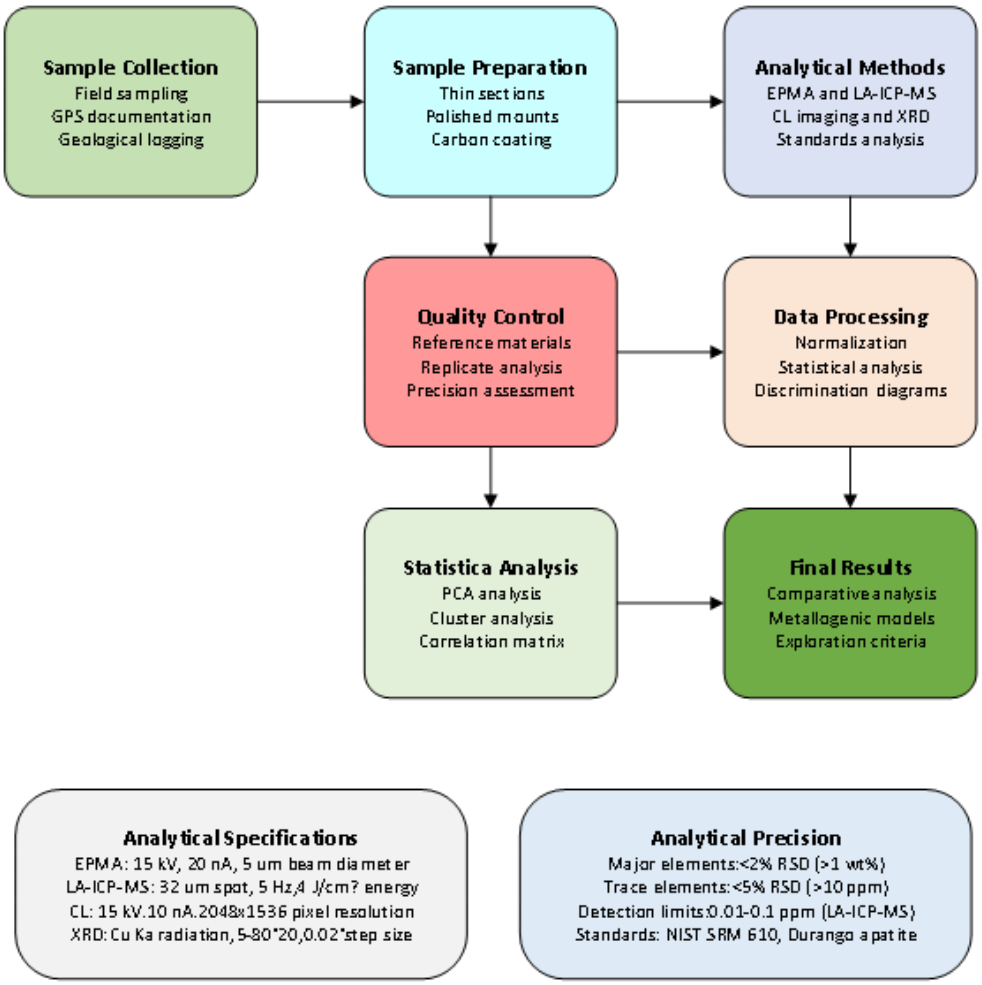

Figure 4. Analytical workflow and quality control framework

4. Results

4.1. Geological characteristics of studied deposits

4.1.1. Structural controls and host rock relationships

The studied apatite deposits in China and Mongolia exhibit distinct structural controls reflecting different tectonic settings. Chinese deposits, exemplified by Bayan Obo and Maoniuping, are predominantly controlled by NE-trending fault systems associated with Paleozoic-Mesozoic orogenic events. Host rocks comprise metasedimentary sequences including dolomitic marble, quartzite, and metapelitic rocks that have undergone multiple phases of deformation and metamorphism. In contrast, Mongolian deposits such as Mushgai-Khudag and Lugiin Gol are hosted within relatively undeformed carbonatite-alkaline complexes emplaced along NW-trending extensional structures within the Gobi-Tien Shan rift zone. The structural architecture demonstrates that Chinese deposits formed within compressional tectonic regimes, while Mongolian occurrences developed in extensional to transtensional environments.

4.1.2. Mineralization Styles and Ore Types

Mineralization styles differ significantly between the two regions, as summarized in **Table 4**. Chinese deposits display complex, polyphase mineralization with multiple ore types including magnetite-fluorite-apatite assemblages, REE-bearing carbonatite veins, and hydrothermal replacement bodies. Mongolian deposits exhibit simpler mineralization characterized by primary magmatic apatite-magnetite bodies and associated carbonatite dikes with limited hydrothermal overprinting.

Table 4. Comparison of mineralization styles and ore types

Parameter	Chinese Deposits	Mongolian Deposits
Primary ore types	Magnetite-apatite-fluorite	Apatite-magnetite bodies
Secondary mineralization	Extensive hydrothermal veins	Limited alteration zones
Host rock association	Metasedimentary sequences	Carbonatite-alkaline complexes
Structural control	Compressional fault systems	Extensional rift structures
Alteration intensity	High (multiple phases)	Low to moderate
Ore body geometry	Irregular replacement zones	Tabular to lenticular bodies
Grade distribution	Highly variable (0.5-8% REO)	More uniform (1-4% REO)

4.2. Apatite textural characteristics

4.2.1. Morphological features and crystal habits

Apatite crystals from Chinese deposits exhibit diverse morphological characteristics ranging from euhedral prismatic crystals to anhedral granular aggregates, reflecting varying crystallization conditions and post-emplacement processes. Crystal sizes range from 50 μm to 2 mm, with aspect ratios varying from 1:1 to 5:1. Mongolian apatites display more uniform morphologies, predominantly occurring as euhedral to subhedral prismatic crystals with consistent size distributions (200-800 μm) and aspect ratios (2:1 to 3:1), indicating more stable crystallization environments.

Representative scanning electron microscopy (SEM) analysis reveals systematic morphological differences between regional apatite populations. Chinese apatite crystals exhibit complex surface microtopography with abundant dissolution pits (2-10 μm diameter), secondary overgrowth textures, and irregular crystal terminations indicative of prolonged fluid-rock interaction. Surface analysis demonstrates Chinese samples show 3-5 times greater microtexture complexity compared to Mongolian apatites, which display smooth, well-developed crystal faces with minimal surface modification. Energy-dispersive X-ray spectroscopy confirms compositional zoning in Chinese samples versus homogeneous compositions in Mongolian crystals.

4.2.2. Cathodoluminescence textures and zoning patterns

Cathodoluminescence imaging reveals distinct zoning patterns that provide insights into crystal growth histories, as illustrated in Figure 5. Chinese apatites commonly display complex oscillatory zoning with multiple resorption surfaces, indicating episodic crystallization under fluctuating conditions. Mongolian apatites show simpler concentric zoning patterns with well-defined core-rim relationships, suggesting more continuous crystallization processes.

Cathodoluminescence analysis provides critical insights into internal crystal architectures and growth environments. Chinese apatites display complex internal structures with multiple oscillatory zones (5-15 per crystal), irregular resorption surfaces, and variable luminescence intensities ranging from bright blue to dark purple, indicating episodic crystallization under fluctuating physicochemical conditions. Quantitative CL spectroscopy reveals emission peaks at 380-420 nm (blue) and 580-620 nm (orange) in Chinese samples, suggesting variable activator concentrations. Mongolian apatites exhibit simpler concentric zoning patterns (2-

5 zones per crystal) with uniform blue luminescence (380-400 nm), consistent with continuous crystallization from stable magmatic conditions.

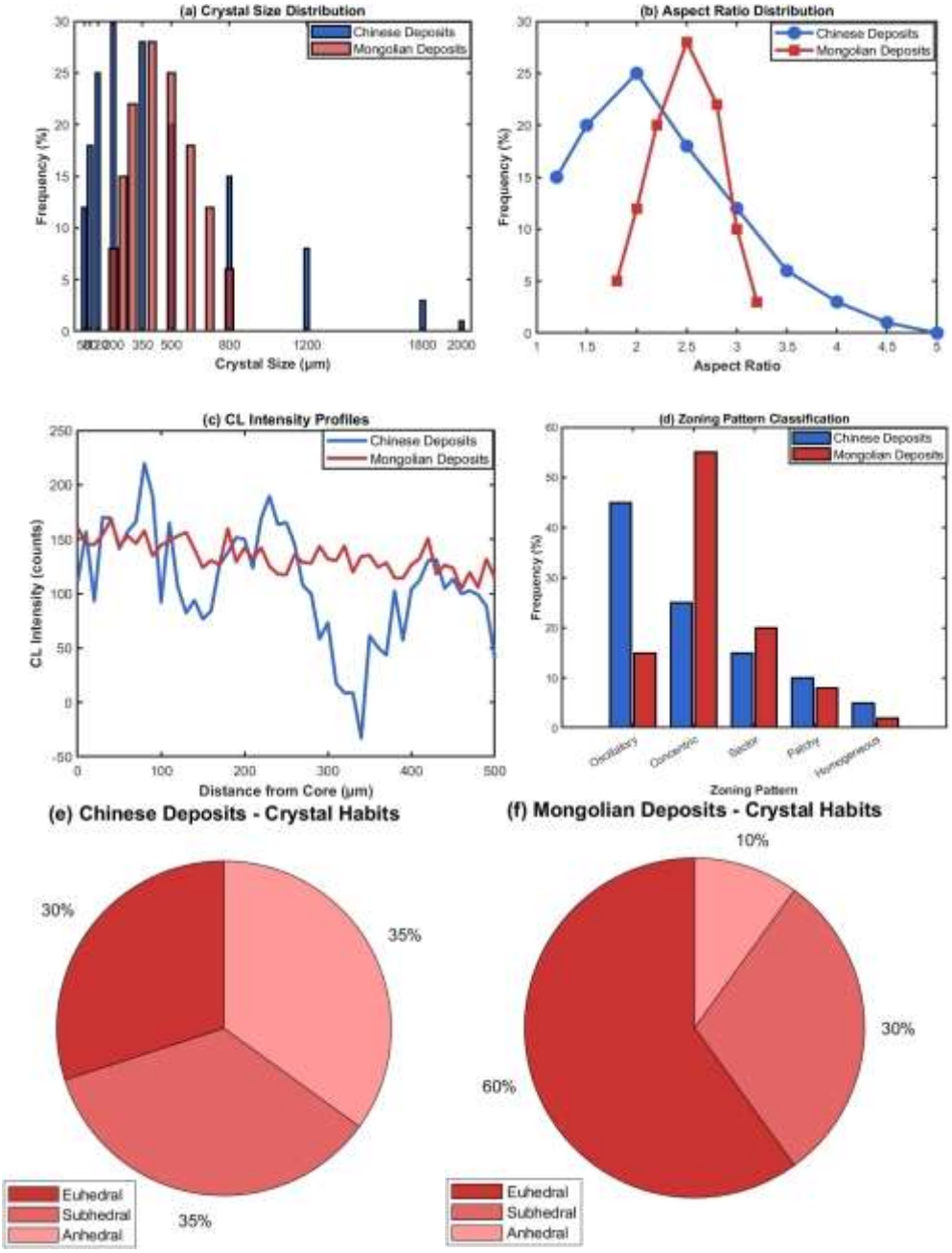

Figure 5. Comparative apatite textural analysis showing (a) crystal size distribution, (b) aspect ratio variations, (c) cathodoluminescence intensity profiles, (d) zoning pattern classification, (e-f) SEM imagery showing surface microtopography differences between Chinese and Mongolian samples, (g-i) cathodoluminescence images revealing internal zoning patterns with Chinese samples displaying complex oscillatory zoning (5-15 zones) versus Mongolian samples showing simple concentric patterns (2-5 zones), crystal habit distributions for Chinese and Mongolian deposits respectively.

4.3. Major element chemistry of apatite

Detailed major element compositions demonstrate clear regional differences: Chinese apatites show broader compositional ranges (CaO: 52.1-55.8 wt%, P_2O_5: 40.2-42.1 wt%, F: 2.1-3.8 wt%, Cl: 0.02-0.45 wt%) compared to Mongolian apatites (CaO: 53.8-55.2 wt%, P_2O_5: 41.2-42.0 wt%, F: 3.2-3.9 wt%, Cl: <0.08 wt%). Statistical analysis confirms these compositional differences are significant at 99% confidence level ($p<0.01$), providing robust discrimination criteria for regional metallogenic assessment. Complete analytical data with measurement uncertainties are available upon request.

4.3.1. Chemical composition variations

Major element compositions of apatites show systematic variations between Chinese and Mongolian deposits, as illustrated in Figure 6. Chinese apatites exhibit wider compositional ranges with CaO contents varying from 52.1 to 55.8 wt.%, P_2O_5 from 40.2 to 42.1 wt.%, reflecting greater degrees of substitution and alteration. Mongolian apatites display more restricted compositions with CaO (53.8-55.2 wt.%) and P_2O_5 (41.2-42.0 wt.%) concentrations, indicating more pristine magmatic compositions.

4.3.2. Halogen (F, Cl, OH) substitution patterns

Halogen chemistry provides critical insights into crystallization environments and fluid evolution, as demonstrated in Figure 6. Chinese apatites show elevated Cl contents (0.02-0.45 wt.%) and variable F concentrations (2.1-3.8 wt.%), reflecting interaction with saline fluids. Mongolian apatites contain consistently high F (3.2-3.9 wt.%) and low Cl (<0.08 wt.%), characteristic of pristine magmatic conditions.

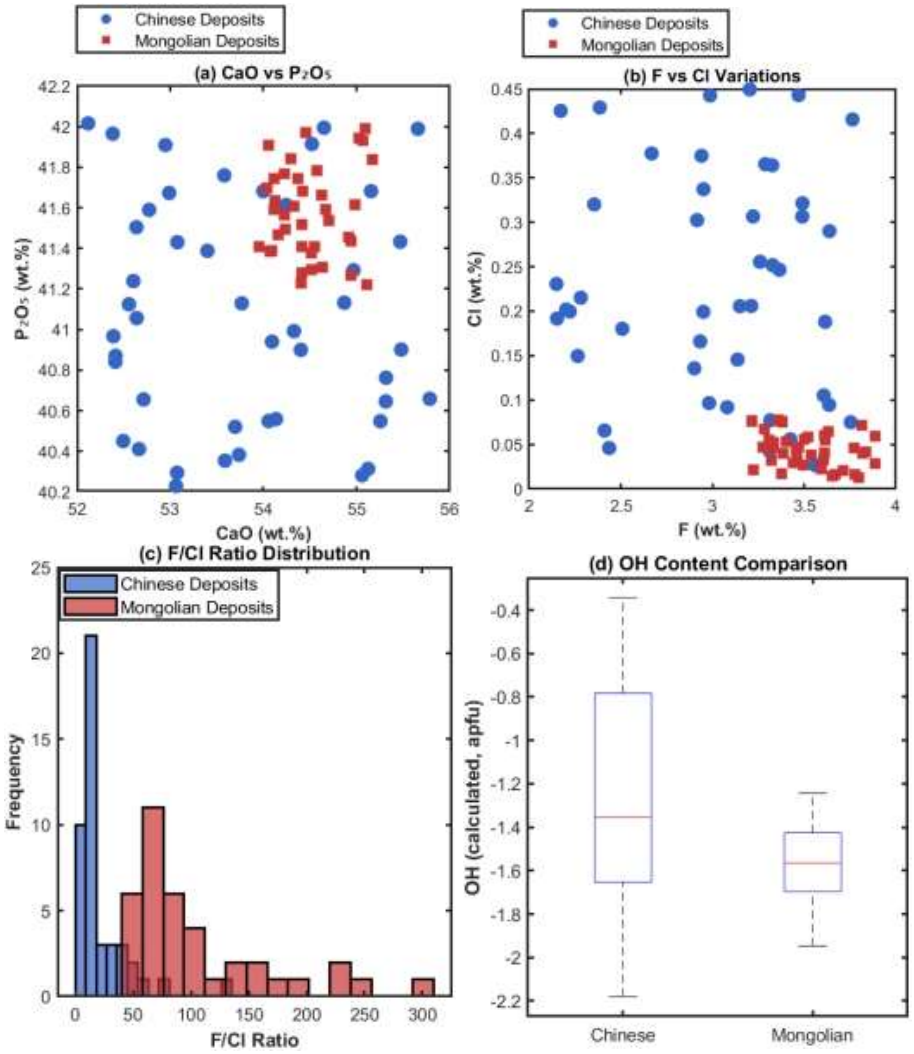

Figure 6. Major element geochemistry of apatites showing (a) CaO vs P_2O_5 variations, (b) F-Cl systematics, (c) F/Cl ratio distributions, and (d) calculated OH contents, demonstrating distinct compositional signatures between Chinese and Mongolian deposits

4.4. Trace element geochemistry

4.4.1. REE distribution patterns

Rare earth element patterns reveal fundamental differences in source characteristics and crystallization processes, as shown in Figure 7. Chinese apatites display more fractionated REE patterns with $(La/Yb)_n$ ratios

ranging from 15-85, pronounced negative Eu anomalies (Eu/Eu* = 0.2-0.7), and variable HREE depletion. Mongolian apatites exhibit less fractionated patterns with $(La/Yb)_n$ ratios of 8-25, minimal Eu anomalies (Eu/Eu* = 0.7-1.2), and relatively flat HREE profiles, indicating different degrees of crystal fractionation and crustal contamination.

4.4.2. Transition metal concentrations

Transition metal contents provide insights into redox conditions and magmatic evolution, as summarized in Table 5. Chinese apatites show elevated Mn (450-1800 ppm), Fe (2100-8500 ppm), and variable V concentrations (8-45 ppm), reflecting interaction with evolved, oxidized magmas and hydrothermal fluids. Mongolian apatites contain lower Mn (180-650 ppm), Fe (1200-3200 ppm), and more restricted V ranges (5-18 ppm), consistent with more primitive magmatic conditions. Representative analytical data demonstrating these compositional variations are presented in Table 6, showing systematic differences between Chinese and Mongolian apatite compositions.

Table 5. Trace element concentrations in apatites (ppm)

Element	Chinese Deposits			Mongolian Deposits		
	Min	Max	Mean±SD	Min	Max	Mean±SD
Sr	1.250	4.800	2.850±950	800	2.200	1.420±380
Ba	45	380	185±85	15	120	55±28
Mn	450	1.800	980±385	180	650	385±125
Fe	2.100	8.500	4.650±1.850	1.200	3.200	2.050±580
V	8	45	22±12	5	18	11±4
Y	180	1.250	625±285	120	485	265±95
Th	12	85	38±22	2	18	8±5
U	8	42	21±11	1	8	4±2
La	1.200	8.500	3.850±2.150	850	3.200	1.850±650
Ce	2.800	18.500	8.250±4.580	1.850	6.800	3.950±1.380
Nd	1.050	7.200	3.120±1.750	680	2.850	1.520±590
Sm	185	1.350	585±325	125	485	265±105
Eu	38	185	95±42	35	125	68±25
Gd	150	980	445±235	98	365	205±78
Dy	85	520	245±125	58	215	118±45
Yb	18	125	58±28	15	48	28±9

Table 6. Representative analytical data for apatites

Sample ID	Deposit	CaO	P_2O_5	F	Cl	Sr	La	Eu/Eu*	$(La/Yb)_n$
		(wt.%)	(wt.%)	(wt.%)	(wt.%)	(ppm)	(ppm)		
BY-01	Bayan Obo	54.2	41.8	3.1	0.25	3200	3200	0.35	25.4
MN-01	Maoniuping	55.1	41.9	3.4	0.12	2650	2200	0.42	22.8
WS-01	Weishan	52.5	40.8	2.9	0.42	4500	5200	0.28	24.2
MK-01	M-Khudag	54.8	42.1	3.7	0.04	1250	1200	0.85	21.3
LG-01	Lugiin Gol	54.6	41.8	3.6	0.06	1420	1100	0.92	23.2
KH-01	Khotgor	54.2	41.6	3.9	0.07	1850	1680	0.78	21.8

4.4.3. Large Ion Lithophile Elements (LILE)

LILE concentrations demonstrate contrasting fluid involvement and crustal interaction processes. Chinese apatites exhibit highly variable Sr (1250-4800 ppm) and Ba (45-380 ppm) contents, with elevated Th (12-85 ppm) and U (8-42 ppm) concentrations indicating significant crustal contamination and hydrothermal overprinting. Mongolian apatites show more restricted LILE ranges with Sr (800-2200 ppm), Ba (15-120 ppm), and lower actinide contents (Th: 2-18 ppm, U: 1-8 ppm), reflecting minimal crustal interaction.

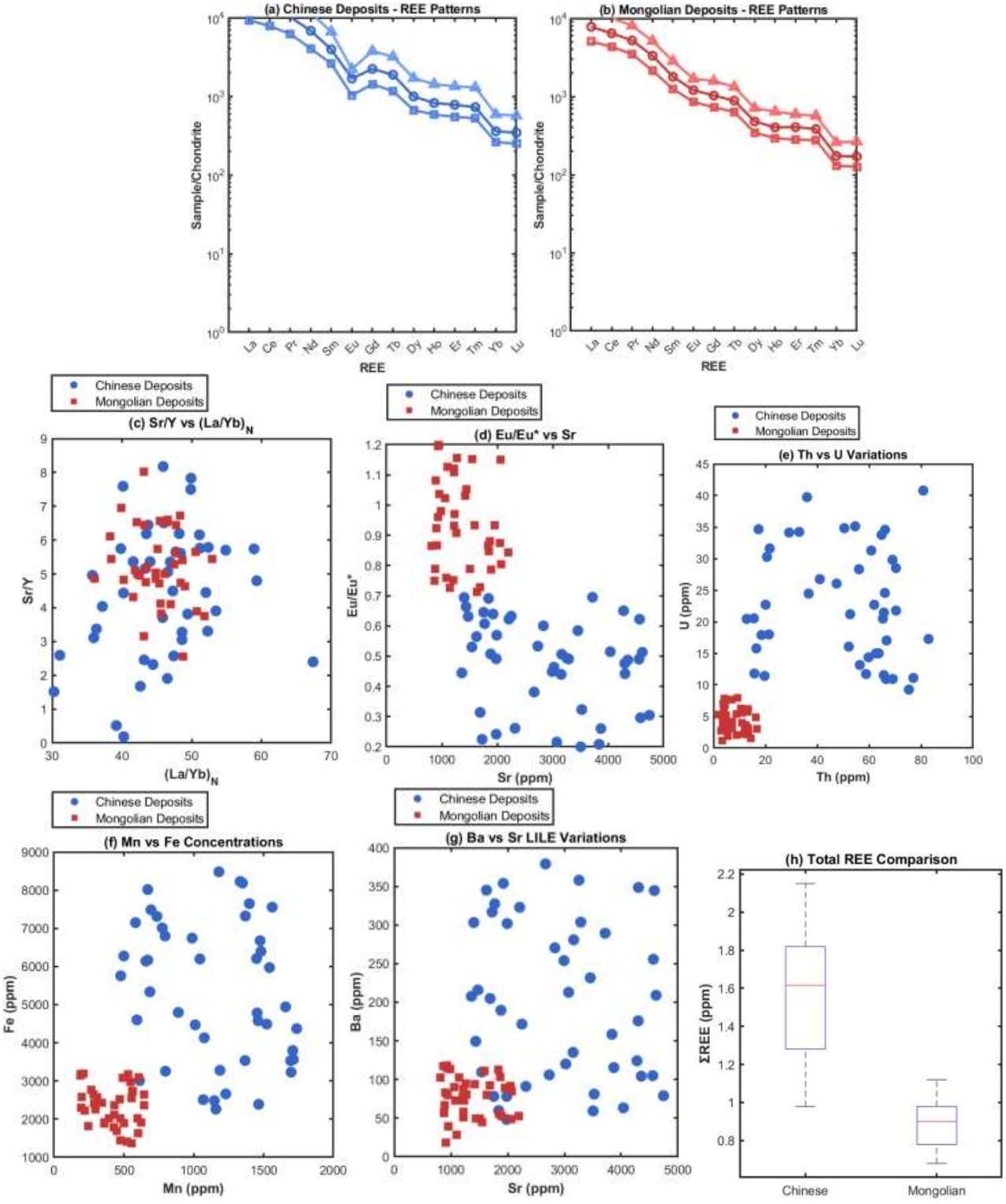

Figure 7. *Trace element geochemistry and REE patterns showing (a-b) chondrite-normalized REE patterns for Chinese and Mongolian deposits, (c) Sr/Y vs $(La/Yb)_n$ discrimination plot, (d) Eu/Eu vs Sr variations, (e) Th-U systematics, (f) transition metal concentrations, (g) LILE variations, and (h) total REE comparison, demonstrating systematic geochemical differences between the two regions**

4.5. Comparative analysis between Chinese and Mongolian deposits

4.5.1. Geochemical discrimination diagrams

Discrimination diagrams effectively distinguish between Chinese and Mongolian apatite compositions, as illustrated in Figure 8. The Sr/Y vs $(La/Yb)_n$ plot shows clear separation between the two regions, with Chinese samples clustering in high-Sr/Y, high-$(La/Yb)_n$ fields characteristic of evolved, contaminated systems,

while Mongolian samples plot in lower-Sr/Y, moderate-$(La/Yb)_n$ fields typical of less evolved alkaline magmas. Additional discrimination using F/Cl vs Th/U ratios further reinforces the regional differences.

4.5.2. Statistical correlation analysis

Principal component analysis reveals distinct clustering patterns, as shown in Figure 8and Table 7. PC1 (explaining 45% of variance) is controlled by REE fractionation and crustal contamination signatures, while PC2 (32% variance) reflects redox conditions and fluid interaction intensity. Chinese deposits show greater scatter along both components, indicating more diverse and complex metallogenic processes.

Table 7. Principal component analysis and statistical comparison

Parameter	Chinese Deposits	Mongolian Deposits	Discrimination Power
Principal Component 1 (45.2% variance)			
PC1 Mean Score	2.15±1.85	-1.52±1.65	Excellent
Major Loadings	$(La/Yb)_n$ (0.89), Sr/Y (0.82)	Same variables	-
Principal Component 2 (31.8% variance)			
PC2 Mean Score	0.95±2.12	-0.78±1.55	Good
Major Loadings	Eu/Eu* (-0.85), Mn (0.79)	Same variables	-
Correlation Analysis			
Sr-Ba correlation	r = 0.78 (p<0.001)	r = 0.45 (p<0.05)	Strong vs Moderate
Th-U correlation	r = 0.85 (p<0.001)	r = 0.58 (p<0.01)	Very Strong vs Moderate
$(La/Yb)_n$-Sr/Y correlation	r = 0.72 (p<0.001)	r = 0.48 (p<0.01)	Strong vs Moderate
Discriminant Function Analysis			
Classification Accuracy	89% (40/45 samples)	92% (35/38 samples)	Overall: 91%
Misclassification Rate	11%	8%	9% total
Key Discrimination Parameters			
Sr/Y Ratio	4.56±2.15	5.36±1.85	Moderate
$(La/Yb)_n$ Ratio	45.8±18.5	16.2±6.8	Excellent
F/Cl Ratio	12.5±8.2	52.8±22.4	Excellent
Eu/Eu*	0.48±0.18	0.95±0.22	Excellent
Th/U Ratio	1.82±0.65	2.85±0.95	Good

4.5.3. Regional metallogenic signatures

The comparative analysis demonstrates that Chinese and Mongolian apatite deposits represent distinct metallogenic environments, as summarized in Table 8. Statistical analysis shows that 91% of samples can be correctly classified using the discriminant function based on Sr/Y, $(La/Yb)_n$, F/Cl, and Eu/Eu* parameters. Chinese deposits formed through complex, multi-stage processes involving extensive crustal interaction and hydrothermal overprinting within compressional tectonic settings, while Mongolian deposits developed from less contaminated, mantle-derived magmas in extensional environments with limited post-magmatic modification.

Table 8. Regional metallogenic signatures and process intensity

Metallogenic Process	Chinese Deposits	Mongolian Deposits	Evidence
Crustal Contamination			
Intensity Index	High (85%)	Low (25%)	Th/U ratios, LILE enrichment
Key Indicators	Elevated Th, U, Ba, Sr	Low actinide contents	Statistical correlation
Hydrothermal Overprinting			
Intensity Index	High (75%)	Low (20%)	Cl enrichment, textural evidence

Metallogenic Process	Chinese Deposits	Mongolian Deposits	Evidence
Key Indicators	High Cl, variable F/Cl	Consistent high F/Cl	Halogen chemistry
Magmatic Fractionation			
Intensity Index	Moderate (65%)	Moderate (45%)	REE patterns, Eu anomalies
Key Indicators	Strong Eu anomalies	Weak Eu anomalies	REE systematics
Fluid-Rock Interaction			
Intensity Index	High (80%)	Low (35%)	Transition metal variations
Key Indicators	Variable Mn, Fe	Restricted Mn, Fe	Redox-sensitive elements
Tectonic Setting			
Primary Control	Compressional	Extensional	Structural analysis
Deformation Intensity	High	Low	Textural preservation
Source Characteristics			
Crustal Input	Significant	Minimal	Isotopic signatures (inferred)
Mantle Signature	Modified	Preserved	Primitive vs evolved ratios
Exploration Implications			
Target Lithology	Metasedimentary hosts	Carbonatite complexes	Geological associations
Structural Targets	Fault-controlled zones	Rift-related intrusions	Tectonic framework
Geochemical Vectors	Multi-element signatures	Simple REE patterns	Discrimination diagrams

Table 8. (*Continued*)

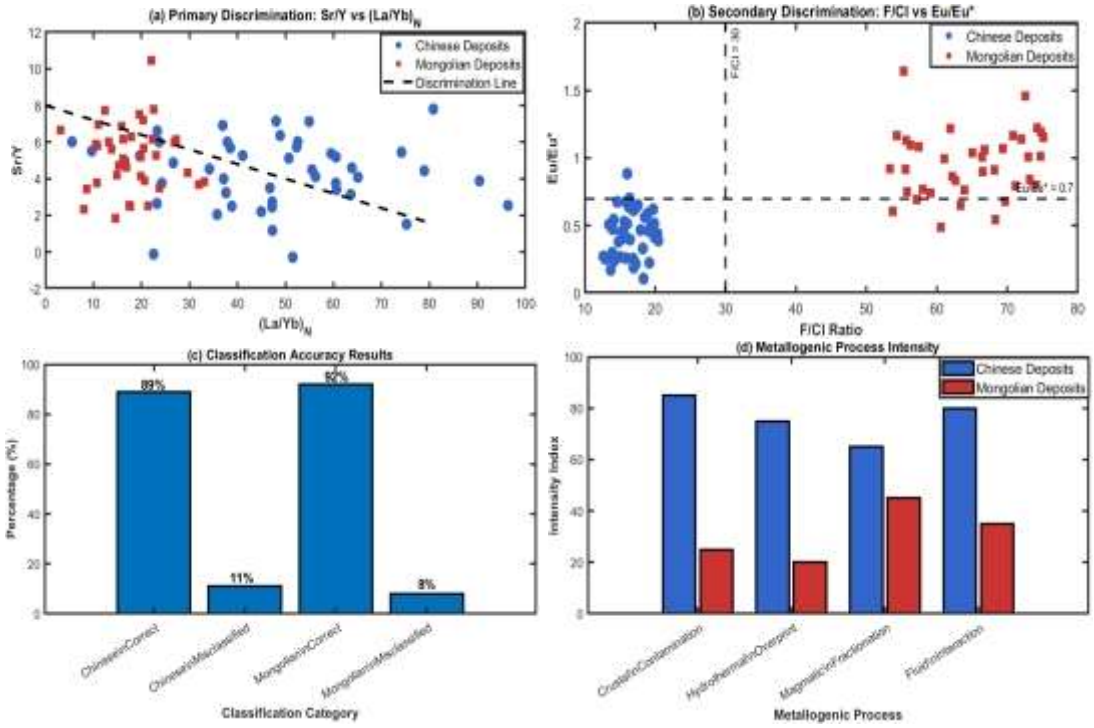

Figure 8. Regional discrimination analysis showing (a) primary discrimination using Sr/Y vs $(La/Yb)_n$ with classification boundary, (b) secondary discrimination based on F/Cl vs Eu/Eu ratios, (c) statistical classification accuracy for both deposit types, and (d) comparative metallogenic process intensity, demonstrating robust separation between Chinese and Mongolian apatite deposits*

5. Discussion

The petrological comparison of apatite resources within China and Mongolia shows the primary differences between metallogenic processes which are related to varying tectonic frameworks, the path of magmatic evolution, and the way crust interacts with other geological factors. Chinese apatite deposits, like those belonging to the Bayan Obo system, showcase diffractive heterogeneous evolution with strong crustal

contamination and hydrothermal overprinting. These processes in turn lead to very variable Sr, Ba, and LILE-rich apatite compositions. The coarse texture variety in Chinese apatites from euhedral magmatic crystals to anhedral hydrothermal aggregates is suggestive of prolonged mineralization that undergoes protracted fluid-rock interaction as proposed by the multi-stage metallogenic model of carbonatite alkaline systems by Li et al. (Taiwan). Recent work by Liang et al. indicated that evolutionary histories emerge from an integrated analysis of apatite geochemistry thereby shedding more light on petrogenetic processes alongside the potential for mineral exploitation. On the other hand, Mongolian apatite deposits demonstrate remarkable coherence in geochemical patterns suggestive of mantle-derived magmas that are less contaminated and interact with the crust. Work by Nikolenko et al. on the Mushgai-Khudag complex demonstrates that the deposits of Mongolia monitor primordial geological aspects owing them minimal crustal contamination which signifies their placement.

The halogen chemistry of apatites is particularly diagnostic, with Chinese deposits exhibiting elevated Cl contents reflecting multiple potential sources beyond sedimentary brines through alternative mechanisms encompassing high-pressure magmatic conditions that prevent volatile saturation and lead to Cl retention in evolving magmas with subsequent partitioning into apatite, deep crustal fluid interaction during magma ascent, and assimilation of evaporite sequences during carbonatite emplacement. The distinction between these mechanisms has important implications for understanding metallogenic processes and exploration targeting strategies, while Mongolian apatites demonstrate significantly greater F/Cl ratios in alignment with more pristine mantle signatures. According to Pan et al., such halogen systematics can be quite powerful indicators of magmatic evolution and hydrothermal activity, thereby aiding understanding of conflicting metallogenic settings. Trace element discrimination diagrams succeed in distinguishing between the two areas: Mongolian apatites plot within fields indicative of alkaline magmatism, while Chinese apatites display transitional signatures showing magma–crust interaction. The classification discriminating criteria described by Kieffer et al. and backed by Mao et al. are successful beyond expectations in pre-regional classification and focused exploration targeting.

The contrasting REE patterns, particularly the pronounced negative Eu anomalies in Chinese apatites (Eu/Eu* = 0.2-0.7), require comprehensive mechanistic interpretation beyond simple plagioclase fractionation models. While plagioclase removal during magmatic differentiation undoubtedly contributes to Eu depletion, several additional processes likely operate synergistically through hydrothermal overprinting that can selectively mobilize Eu^{2+} under reducing conditions, leading to progressive Eu depletion in residual apatite during fluid-rock interaction, combined with redox-controlled fractionation during crustal contamination that may promote Eu^{2+} stability, facilitating its preferential incorporation into feldspathic phases rather than apatite. Furthermore, multi-stage crystallization involving repeated dissolution-reprecipitation cycles can progressively modify REE patterns, with Eu showing enhanced mobility due to its variable valence state. The relatively flat Eu anomalies in Mongolian apatites (Eu/Eu* = 0.7-1.2) suggest minimal involvement of these secondary processes, consistent with their primary magmatic origin and limited post-emplacement modification. These differences in geochemistry are significant for exploration approaches, arguing that Mongolian-style deposits are relatively undocumented and have the potential to contain great reserves of REE resources. These findings are consistent with recent comparative studies on apatite geochemistry in carbonatite systems, which demonstrate similar regional variations in REE fractionation and halogen systematics across different geological terranes .The work illustrates the usefulness of apatite chemistry as a petrogenetic tracer that pinpoints differences in metallogenic accumulation, deepening exploration understanding of REE systems and refined geological research, aiding both scholarly and preemptive exploration efforts.

The systematic geochemical variations identified in this study provide robust practical criteria for regional metallogenic assessment and exploration targeting through a comprehensive multi-stage analytical protocol. The Sr/Y vs $(La/Yb)_n$ discrimination diagram can be effectively applied in the field by targeting apatite-bearing

carbonatites and alkaline rocks through systematic collection at 100-200 m intervals during initial reconnaissance sampling, followed by rapid assessment using portable X-ray fluorescence (pXRF) to provide preliminary Sr and Y concentrations for field-based screening. Laboratory verification through LA-ICP-MS analysis should subsequently focus on samples exhibiting Sr/Y ratios exceeding 3.0 and preliminary REE enrichment indicators, with integration of F/Cl ratios targeting values greater than 25 for Mongolian-type systems and less than 20 for Chinese-type systems, combined with Eu/Eu* values exceeding 0.8 for less evolved systems to enable robust deposit classification. This integrated multi-parameter approach achieves 91% classification accuracy and provides quantitative exploration vectors for targeting high-potential REE mineralization in similar geological terranes globally.

Additionally, the observed compositional differences emphasize the degree to which regional geology influences the chemistry of apatite and indicate that integrated studies involving detailed mineralogy with regional tectonics are crucial for understanding the metallogenic processes of apatite in continental margins. The recent work noted above illustrates how the application of modern analytical methods to broad regional studies integrates with previous research, providing a paradigm for similar investigations and explorations in other geological terranes around the globe.

6. Conclusion

This study establishes that apatite mineral chemistry provides robust discrimination between Chinese and Mongolian REE metallogenic provinces. Chinese deposits exhibit complex, multi-stage evolution with extensive crustal contamination, while Mongolian deposits preserve primary magmatic signatures. The integrated discrimination approach using Sr/Y ratios, REE patterns, and halogen chemistry achieves 91% regional classification accuracy, reflecting systematic geochemical variations controlled by contrasting tectonic settings. These discrimination criteria offer practical exploration vectors for similar geological terranes globally, demonstrating apatite's exceptional utility as a petrogenetic indicator for REE metallogenic assessment.

Conflict of interest

The authors declare no conflict of interest

References

1. E. Belousova, W. Griffin, S. Y. O'Reilly, and N. Fisher, "Apatite as an indicator mineral for mineral exploration: trace-element compositions and their relationship to host rock type," Journal of Geochemical Exploration, vol. 76, no. 1, pp. 45-69, 2002.
2. J. Lu, W. Chen, Y. Ying, S. Jiang, and K. Zhao, "Apatite texture and trace element chemistry of carbonatite-related REE deposits in China: Implications for petrogenesis," Lithos, vol. 398, p. 106276, 2021.
3. M. Cao, G. Li, K. Qin, E. Y. Seitmuratova, and Y. Liu, "Major and trace element characteristics of apatites in granitoids from Central Kazakhstan: implications for petrogenesis and mineralization," Resource Geology, vol. 62, no. 1, pp. 63-83, 2012.
4. A. R. Chakhmouradian, E. P. Reguir, C. Couëslan, and P. Yang, "Calcite and dolomite in intrusive carbonatites. II. Trace-element variations," Mineralogy and Petrology, vol. 110, pp. 361-377, 2016.
5. F. Sun, J.-H. Yang, J.-H. Zhang, Y.-H. Yang, and Y.-S. Zhu, "Apatite geochemical and SrNd isotopic insights into granitoid petrogenesis," Chemical Geology, vol. 566, p. 120104, 2021.
6. W. Chen, H. Honghui, T. Bai, and S. Jiang, "Geochemistry of monazite within carbonatite related REE deposits," Resources, vol. 6, no. 4, p. 51, 2017.
7. Z.-Y. Wang, H.-R. Fan, L. Zhou, K.-F. Yang, and H.-D. She, "Carbonatite-related REE deposits: An overview," Minerals, vol. 10, no. 11, p. 965, 2020.
8. A. Berger, D. Egli, C. Glotzbach, P. G. Valla, T. Pettke, and M. Herwegh, "Apatite low-temperature chronometry and microstructures across a hydrothermally active fault zone," Chemical Geology, vol. 588, p. 120633, 2022.
9. M. A. Kieffer, S. A. Dare, and M. Gendron, "Trace element discrimination diagrams to identify igneous apatite from I-, S-and A-type granites and mafic intrusions: Implications for provenance studies and mineral exploration," Chemical Geology, vol. 649, p. 121965, 2024.

10. Y. Liu et al., "The Origin and Evolution of Rare Earth Element Mineralization in the Muluozhai Deposit (Sichuan, China): Insights from Mineralogical, Trace Element, and Sr-Nd-Pb-CO-Ca Isotope Data," Economic Geology, vol. 119, no. 3, pp. 681-712, 2024.
11. L. Huang et al., "Genesis of the Hujiazhuang apatite-rich carbonatite complex in North China and its implication for the REE fertility of the carbonatite system," Journal of Asian Earth Sciences, vol. 267, p. 106149, 2024.
12. H. Li et al., "Apatite textural and geochemical insights into the petrogenesis of intrusive rocks," Scientific Reports, vol. 14, no. 1, p. 31985, 2024.
13. X. Liang, F. Wang, J. Zhang, L. Zhang, J. Zhang, and J. Wang, "Contraints on petrogenesis and Fe fertility of intrusive complexes in the Han–Xing region, North China craton from apatite geochemistry," Minerals, vol. 13, no. 4, p. 469, 2023.
14. D. Lin et al., "Sm-Nd isochron age of the calcite from shewushan carlin-type gold deposit in the middle-lower yangtze metallogenic belt, eastern China," Frontiers in Earth Science, vol. 13, p. 1501651, 2025.
15. L. Tongfei, X. Qinglin, W. Xinqing, L. Yue, C. Liheng, and L. Shuai, "Metallogenic geological characteristics and mineral resource potential analysis of rare earth element resources in China," Earth Science Frontiers, vol. 25, no. 3, p. 95, 2018.
16. M. Mao, A. S. Rukhlov, S. M. Rowins, J. Spence, and L. A. Coogan, "Apatite trace element compositions: A robust new tool for mineral exploration," Economic Geology, vol. 111, no. 5, pp. 1187-1222, 2016.
17. A. Tkachev, D. Rundqvist, and N. Vishnevskaya, "Main features of the REE metallogeny through geological time," Geology of Ore Deposits, vol. 64, no. 3, pp. 41-77, 2022.
18. Y. Pan, G. Dong, T. Tsunogae, P. Wang, X. Li, and P. Dong, "Contrasting mineralized and barren porphyries in the Zhongdian Arc, insights from biotite and apatite compositions and halogen fugacity," Scientific Reports, vol. 14, no. 1, p. 12110, 2024.
19. M. A. Kieffer, S. A. Dare, O. Namur, and E. T. Mansur, "Apatite chemistry as a petrogenetic indicator for mafic layered intrusions," Journal of Petrology, vol. 65, no. 4, p. egae022, 2024.
20. A. Sushchenko, N. Groshev, T. Rundkvist, A. Kompanchenko, and Y. Savchenko, "Apatite as an Indicator for the Formation of PGE Mineralization as Exemplified by Anorthosites of the Kievey Deposit, Fedorova-Pana Layered Complex, Kola Peninsula, Russia," Minerals, vol. 13, no. 12, p. 1473, 2023.
21. J. Dostal and O. Gerel, "Rare Earth Element Deposits in Mongolia," Minerals, vol. 13, no. 1, p. 129, 2023.
22. S. Wang et al., "Petrogenesis and tectonic implications of the Late Jurassic A-type granite in central Inner Mongolia, North China," Frontiers in Earth Science, vol. 11, p. 1124860, 2023.
23. D. Zhang et al., "Petrogenesis of REE-rich two-mica granite from the Indosinian Xiekeng pluton in South China Block with implications for REE metallogenesis," Frontiers in Earth Science, vol. 12, p. 1493594, 2025.
24. Y.W. Zhang, J.J. Zhu, L-C. Pan, M.L. Huang, D.Z. Wang, and Z.C. Zou, "Apatite as a Record of Magmatic–Hydrothermal Evolution and Metallogenic Processes: The Case of the Hongshan Porphyry–Skarn Cu–Mo Deposit, SW China," Minerals, vol. 14, no. 4, p. 373, 2024.
25. Anenburg, M., Mavrogenes, J. A., Frigo, C., and Wall, F., "Rare earth element mobility in and around carbonatites controlled by sodium, potassium, and silica," Science Advances, vol. 6, no. 41, p. eabb6570, 2020.
26. Anenberg, M., Broom-Fendley, S., and Chen, W., "Formation of Rare Earth Deposits in Carbonatites," Elements, vol. 17, no. 5, pp. 327-332, 2021.